Bi et al. Nanoscale Research Letters (2015) 10:345
DOI 10.1186/s11671-015-1054-5

Nanoscale Research Letters
a SpringerOpen Journal

NANO EXPRESS Open Access

Photoreduction of CO_2 on TiO_2/$SrTiO_3$ Heterojunction Network Film

Yongsheng Bi†, Lanlan Zong†, Chen Li, Qiuye Li* and Jianjun Yang

Abstract

Nanotube titanic acid (NTA) network film has a porous structure and large BET surface area, which lead them to possessing high utilization of the incident light and strong adsorption ability. We used NTA as the precursor to fabricate a TiO_2/ $SrTiO_3$ heterojunction film by the hydrothermal method. In the process of the reaction, part of NTA reacted with $SrCl_2$ to form $SrTiO_3$ nanocubes, and the remainder dehydrated to transform to the rutile TiO_2. The ratio of TiO_2 and $SrTiO_3$ varied with the hydrothermal reaction time. SEM and TEM images indicated that $SrTiO_3$ nanocubes dispersed uniformly on TiO_2 film, and the particle size and crystallinity of $SrTiO_3$ nanocubes increased with the reaction time prolonging. The TiO_2/$SrTiO_3$ heterojunction obtained by 1 h showed the best activity for CO_2 photoreduction, where the mole ratio of TiO_2 and $SrTiO_3$ was 4:1. And the photo-conversion efficiency of CO_2 to CH_4 improved remarkably after the foreign electron traps of Pt and Pd nanoparticles were loaded. The highest photocatalytic production rate of CH_4 reached 20.83 ppm/h cm^2. In addition, the selectivity of photoreduction product of CO_2 was also increased apparently when Pd acted as the cocatalyst on TiO_2/$SrTiO_3$ heterojunction film.

Keywords: Nanotube titanic acid; Porous network film; TiO_2/$SrTiO_3$ heterojunction; CO_2 photoreduction; Product selectivity

Background

Nowadays, the fossil fuels are still the main energy resource for our society. However, the shortage of fossil fuels and the growing environmental concerns due to the emission of large amounts of CO_2 during the combustion of fossil fuels have become the global problems. Conversion of CO_2 into useful hydrocarbon fuels is a possible avenue to develop alternative fuels, and prevent the green house effect on the global temperature. For example, the chemical conversion of CO_2 into industrially beneficial compounds is advantageous in terms of green and sustainable chemistry because CO_2 is an inexpensive, nontoxic and abundant C1 feedstock [1]. Particularly, catalytic conversion of CO_2 to hydrocarbon fuels and chemicals have attracted much attention in recent years [2–6].

At the same time, TiO_2-based materials are the most common photocatalysts because of their many advantages. Especially, one-dimensional TiO_2 nanostructures have become of increasing importance in applications of photocatalysis, photoelectron-chemical process, and dye-sensitized solar cells due to their superior properties in comparison with other TiO_2 nanostructured counterparts [7–12]. Besides, TiO_2-based nanomaterials, especially the layered titanate nanotubes, obtained by the hydrothermal method possess the large BET surface area, strong ion-exchange capacity, and strong adsorption ability [13]. The high recombination of the photo-generated charge carriers leads to the low photocatalytic activity of TiO_2-based nanomaterials. In order to overcome this drawback, forming a heterojunction structure by combing TiO_2 with another semiconductor is considered to be one of the efficient ways to suppress the recombination of the photo-excited electron-hole pairs and to enhance the photocatalytic efficiency [14, 15]. $SrTiO_3$ with the perovskite structure is one of semiconductors with a flat band potential lower than that of TiO_2, and it is easily to be formed a heterojunction structure with TiO_2 in the preparation process [16–19]. In this regard, the photo-generated electrons would centralize on the conduction band of TiO_2, and the holes would concentrate on the valence band of $SrTiO_3$

* Correspondence: qiuyeli@henu.edu.cn
†Equal contributors
Key Laboratory for Special Functional Materials, Henan University, Kaifeng 475004, China

under UV light irradiation, and as a result, the recombination efficiency of the photo-generated charge carriers is inhibited, and thereby the photocatalytic activity would be improved [20].

On the basis of above consideration, we intent to fabricate the $TiO_2/SrTiO_3$ heterojunction structure film by the hydrothermal method. Herein, the cubic $SrTiO_3$ was achieved by hydrothermal treatment of the orthorhombic titanic acid in $SrCl_2$ aqueous solution by adjusting pH = 13. Notably, by simply tuning reaction time, the crystallinity, morphology and the amount of $SrTiO_3$ nanostructures can be controlled easily. The $TiO_2/SrTiO_3$ heterostructure film exhibited the good photocatalytic performance for CO_2 photoreduction. In order to further improve the transformation yield, the foreign electron traps of Pt and Pd nanoparticles were loaded on the film by the photoreduction approach. The relationship between the photocatalytic properties of $TiO_2/SrTiO_3$ heterostructure film with their morphology and structure was investigated systematically.

Methods

Preparation of the Film Photocatalysts

Ti foil with a size of 2 cm × 4 cm was put into an autoclave containing a concentrated 10 M NaOH aqueous solution, and then reacted at 120 °C for 24 h. After cooling down, the obtained film was washed with distilled water several times, and then immersed in 0.1 M HCl aqueous solution for 12 h to obtain the titanic acid nanotubes film (TAN). After that, TAN was put into an autoclave containing 80 mL 0.05 M $SrCl_2$ aqueous solution, and the pH value of the solution was adjusted to 13 by NaOH solution. The autoclave was kept at 120 °C for 1 h, 2 h, and 3 h respectively. The as-fabricated films were washed with deionized water several times, and then dried with the stream of N_2. The samples obtained in the different reaction time were denoted as TS1, TS2, and TS3, respectively. In order to further increase the photocatalytic performance, the foreign electron traps of Pt and Pd nanoparticles were deposited on the TS1 surface by photoreduction of H_2PtCl_6 and $PdCl_2$ solution under the irradiation of the high-pressure mercury lamp for 1 h. The obtained products were denoted as TS1-Pt and TS1-Pd.

Characterization

X-Ray powder diffraction (XRD) patterns of the films were measured on a Philips X'Pert Pro X-ray diffractometer (Holland) (Cu *Kα* radiation; 2θ range 5 ~ 70°, step size 0.08°, time per step 1.0 s, accelerating voltage 40 kV, and applied current 40 mA). The morphologies of the samples were taken on SEM (JSM-7100 F, JEOL Co., Japan) and TEM (JEM-2010, JEOL Co., Japan). X-ray photoelectron spectra (XPS) were recorded with a Kratos AXIS Ultra spectrometer (excitation source: monochromatized Al *Kα* ($h\nu$ = 1486.6 eV); voltage 15 kV, current 10 mA). And the C 1 s binding energy of hydrocarbon (284.8 eV) was used as the standard for the correction of charging shift.

Evaluation of Photocatalytic Activity

The photocatalytic reduction of CO_2 was conducted in a flat closed reactor with the inner capacity of 358 mL containing 20 mL 0.1 mol/L $KHCO_3$ solution. The prepared samples were located in the center of the reactor and then the ultra-pure gaseous CO_2 and water vapor was flowed through the reactor for 2 h to achieve the adsorption-desorption equilibrium. Before illumination, the reactor was sealed. The light source was the high pressure Hg lamp with 300 W, and the intensity of the incident light was measured to be 10.4 mW/cm^2. Both sides of the Ti foil have transformed to $TiO_2/SrTiO_3$ heterojunction film, but only one side under the light irradiation took part in the CO_2 photo-reduction reaction. The photocatalytic reaction was typically performed at room temperature for 6 h. The concentration of CO, CO_2, and CH_4 were measured by a gas-chromatography (GC). Moreover, the electrochemical impedance spectroscopy (EIS) properties were measured in 0.05 M Na_2SO_3 aqueous solution using a three-electrode photoelectrochemical cell with TS film as the working electrode, an Ag/AgCl electrode as the reference, and a platinum meshwork as the counter electrode.

Results and Discussion

Phase Structure of the Porous Film

The phase structure of the films was measured by the XRD technique. As illustrated in Fig. 1, curve *a* showed that the titanic acid nanotube (TAN) film belongs to the orthorhombic structure, which is consistent with our

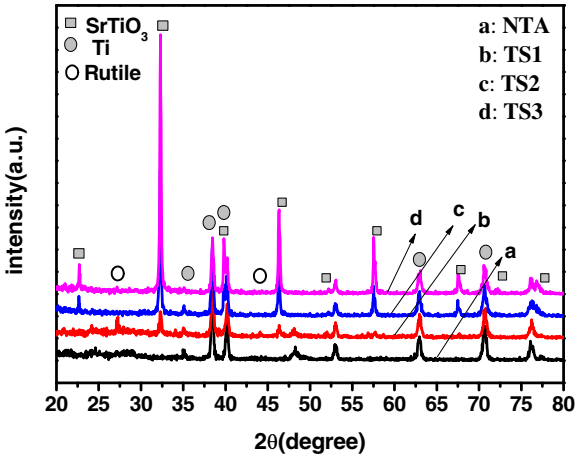

Fig. 1 XRD patterns of film photocatalysts

previous work [21]. There are some characteristic peaks at 38.5°, 40.2°, 63.1°, and 70.7°, which were indexed to the metallic Ti. That indicated only the surface of the Ti foil transformed to TAN after reacting with NaOH, and the interior part still remained as Ti metal. After hydrothermal treatment of TAN film in $SrCl_2$ solution at 120 °C for 1 h, additional diffraction peaks at 22.7°, 32.2°, 46.3°, 57.6°, and 67.8° appeared, which were corresponded to the (100), (110), (200), (211), and (220) crystal planes of cubic $SrTiO_3$, respectively (as shown in curve *b*). This result indicated that part of TAN successfully converted into the cubic $SrTiO_3$. At the same time, two peaks at about 27.46° and 44.08° of rutile TiO_2 appeared, indicating that the residue TAN converted to rutile in the base solution. When the reaction time prolonged to 2 h, the peaks of TiO_2 disappeared, that illustrated TAN transformed into $SrTiO_3$ completely (as shown in curve *c*). As the increase of the reaction time, the peak intensity of $SrTiO_3$ increased by comparing curve b and c, which indicated that the crystallinity of the cubic $SrTiO_3$ improved.

Morphology and Composition Analysis of $TiO_2/SrTiO_3$ Heterostructure

Figure 2 shows the FE-SEM images of TAN and $TiO_2/SrTiO_3$ heterostructure films. From Fig. 2a, we can see that TAN film consisted of a large amount of nanotubes, and many nanotubes intertwined together to form a porous an incompact structure. The diameters of TAN nanotubes were uniform, and their lengths expanded to several micrometers. The inset figure showed that the thickness of TAN film was about 1.6 μm. Figure 2b illustrated that some cubic nanoparticles emerged in TAN films, indicated that part of TAN has transformed to $SrTiO_3$. As the increase of the reaction time, TAN disappeared and transformed to $SrTiO_3$ nanoparticles completely (shown in Fig. 2c). When the reaction time increased to 3 h, the irregular $SrTiO_3$ nanoparticles grew to the regular $SrTiO_3$ nanocubes, indicating that the crystallinity becomes better. The above results were in accordance very well with the XRD results. And the average particle size of $SrTiO_3$ nanocubes in Fig. 2d was about 70–80 nm. To further observe the morphology of $TiO_2/SrTiO_3$ heterojunction strucuture, some powders were peeled off from the film. The TEM images in Fig. 3 showed that, TiO_2 nanotubes and $SrTiO_3$ nanocubes coexisted in the $TiO_2/SrTiO_3$ heterojunction strucuture. The diameter of TiO_2 nanotubes was about 8–10 nm, and $SrTiO_3$ nanocubes were ca. 80 nm, which consisted with the SEM results. From Fig. 3b, we can obviously found that the figure lattice spacing of $SrTiO_3$ nanocubes was regular and clear, indicating that the crystallinity of $SrTiO_3$ was very good. And Fig. 3c showed that TiO2 nanotubes and $SrTiO_3$ nanocubes formed a very closely heterjunction structure, which should be favorable for the separation of the charge carriers. The phase composition of $TiO_2/SrTiO_3$ heterojunction was also measured by XPS techniques (shown in Fig. 3d). The XPS spectrum of Ti 2p was wide and asymmetric, which indicated that there could be more than one chemical state according to the binding energy [20, 22]. Using the XPS Peak fitting program, the Ti 2p XPS spectrum could be fitted to two kinds of chemical states, that was ascribed to Ti^{4+}/TiO_2 and $Ti^{4+}/SrTiO_3$, respectively [23]. The mole ratio of TiO_2 and $SrTiO_3$ was tested to be 4:1.

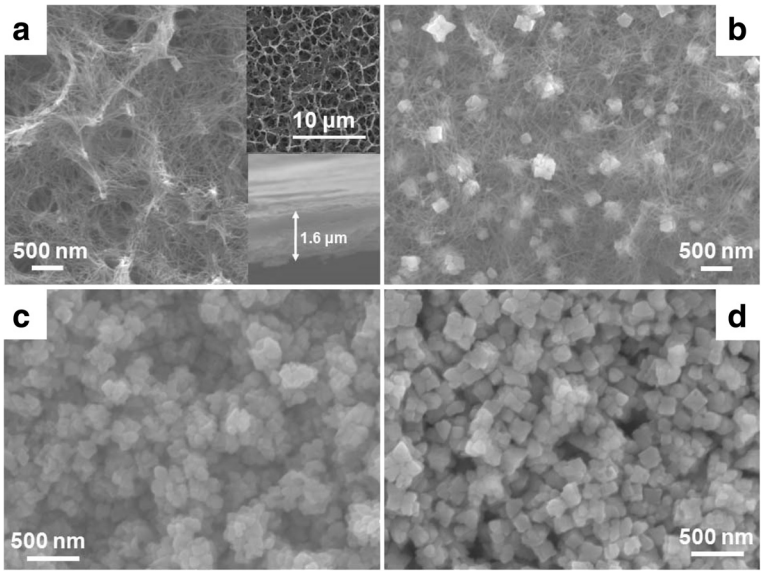

Fig. 2 The top SEM images of the film photocatalysts. **a** NTA. **b** TS1. **c** TS2. **d** TS3. The inset of Fig. 2a shows the large-scale image and the thickness of the film

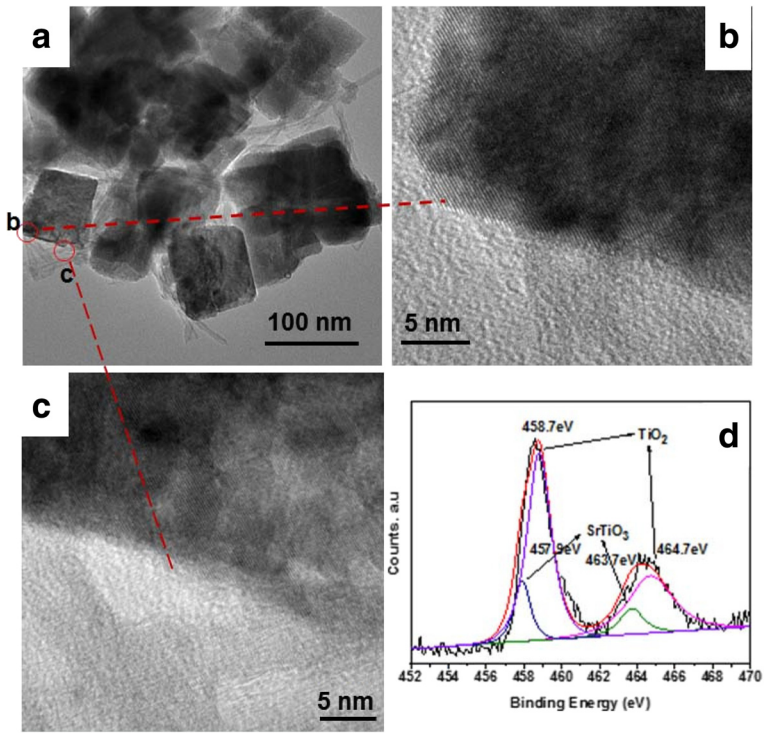

Fig. 3 TEM and HRTEM images $TiO_2/SrTiO_3$ heterojunction (**a**-**c**), XPS spectrum of Ti 2p in TS1 film (**d**)

Photoreduction of CO_2 on $TiO_2/SrTiO_3$ Heterojunction Films

The photo-reduction reaction of CO_2 was selected to evaluate the photocatalytic activity of $TiO_2/SrTiO_3$ heterojunction films. As shown in Fig. 4, the production rate of CH_4 on TS1, TS2, and TS3 films was 3.67, 2.73, and 3.37 ppm/h · cm^2, respectively. From the above XRD and SEM result, we knew that TS1 was $TiO_2/SrTiO_3$ heterojunction films, and the main composition of TS2 and TS3 was $SrTiO_3$. These results indicated that the $TiO_2/SrTiO_3$ heterojunction exhibited the best photocatalytic activity of CO_2 photoreduction to CH_4. The reasons of the high photo-activity of $TiO_2/SrTiO_3$ film can be attributed to three aspects. Firstly, the efficient heterojunction by direct coupling of TiO_2 and $SrTiO_3$ nanostructures during short duration hydrothermal treatment caused the Fermi level to equilibrate and reduced the recombination of charge carriers at the surface of the heterostructure. And thus favored the separation of photogenerated electrons-holes pairs and improved the photo-conversion efficiency [24]. Secondly, the large BET surface areas and strong adsorption capability of the $TiO_2/SrTiO_3$ network structure would facilitate more CO_2 molecules to adsorb, and thus the localized concentration of CO_2 molecules would be higher, which would enhance the photoreduction reaction rate of CO_2 to methane. Thirdly, more light can be scattered or reflected in the porous and incompact structure of the $TiO_2/SrTiO_3$ network film, so the utilization yield of the irradiated light would be improved [25]. Comparison the photoactivity of TS2 and TS3, we found that the photoreduction rate of CO_2 on TS3 was higher, which should be due to the high crystallinity of TS3 nanocubes.

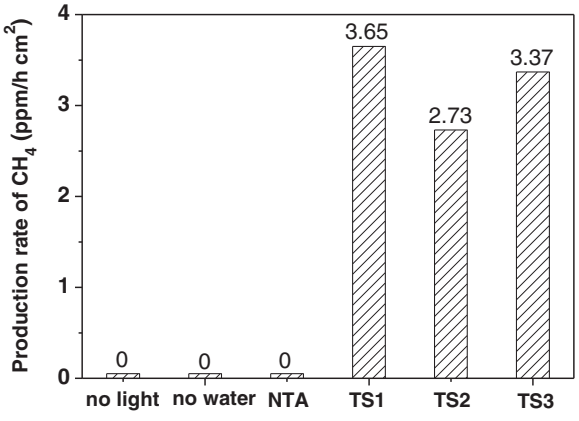

Fig. 4 Photocatalytic production rate of CH_4 on different photocatalyts

As an effective tool for probing the features of surface-modified electrodes, electrochemical impedance spectroscopy (EIS) was employed to analyze the electron transport properties of $TiO_2/SrTiO_3$ (TS) electrodes. As shown in Fig. 5, the impedance arc radius of TS1 was much smaller than TS2 and TS3, and that of TS2 was the largest. EIS spectrum often displays the conductivity of an electrode, and a larger arc radius usually illustrates

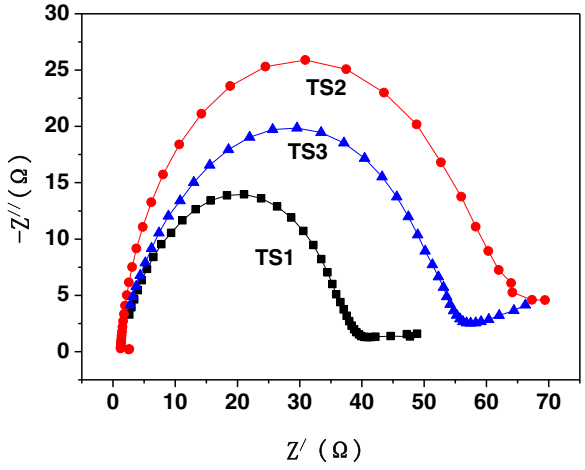

Fig. 5 EIS Nyquist plots of TS1, TS2, and TS3 electrodes under light irradiation

a higher charge transfer resistance [26–28]. So, The EIS results indicated that the separation and transfer efficiency of the photo-generated charge carriers of TS1 was much higher than that of TS2 and TS3, which is consistent very well with their photocatalytic activity.

To confirm the real photocatalytic reduction process of CO_2 to CH_4 on $TiO_2/SrTiO_3$ heterojunction films, some related reference experiments were conducted. When the reaction was preceded in dark, there was no CH_4 detectable, indicating that the photo-excited process of TS film was essential in the photo-reduction of CO_2. When the experiment was conducted in the absence of H_2O, almost no CH_4 was produced. That should be due to no reduce species (H^+) took part in the photo-reduction of CO_2. If we use the NTA nanotube film to replace TS film, there was also no photoactivity. The above comparison experiments illustrated that the conversion of CO_2 to CH_4 on TS films was indeed the photo-reduction process.

Photocatalytic Activity on Pt (or Pd) Loaded $TiO_2/SrTiO_3$ Heterojunction Films

In order to further raise the photocatalytic activity of TS film, Pt and Pd nanoparticles were loaded on TS1 film by the photoreduction method. As shown in Fig. 6, Pt and Pd nanoparticles with the average size of 4–6 nm dispersed uniformly on TiO_2 nanotubes. Due to the similar size of Pt (or Pd) nanoparticles and the TiO_2 nanotube diameters, so it is easily to observe and distinguish the loaded noble metals. However, the particle size of $SrTiO_3$ nanocubes is about 70–80 nm, and the crystallinity of $SrTiO_3$ in TS1 is not very good, and thus the borderline of $SrTiO_3$ nanocubes is not clear, so it is difficult to differentiate the loaded small Pt and Pd nanoparticles. Because Pt and Pd nanoparticles were loaded on TS1 by the photoreduction, they should be dispersed on both TiO_2 nanotubes and $SrTiO_3$ nanocubes. The activity of CO_2 photo-reduction on Pt or Pd loaded $TiO_2/SrTiO_3$ heterojunction films were illustrated in Fig. 7. Compared with the bare TS1 film, the photocatalytic activity for CH_4 and CO production after loading Pt or Pd nanoparticles increased remarkably. The production rate of CH_4 increased from 3.67 to 11.37 and 20.83 ppm/h cm^2 when Pt and Pd loaded on TS1. In the meantime, the production rate of CO increased from 2.93 to 5.38 and 7.49, respectively. Pt or Pd nanoparticles are often used as the co-catalysts to increase the separation efficiency of the photo-generated electron-hole pairs [29, 30]. In this work, they indeed played the important role to enhance the photocatalytic activity for CO_2 reduction. In addition, comparison TS1-Pt and TS1-Pd film, we found that the loaded noble metals played different effect on the enhancement of the photoactivity. When Pt loaded TS1, the production rate of CH_4 increased 2.1 times. While for Pd loaded TS1, it increased 4.7 times, indicating that Pd is more efficient to improve the photoactivity of CH_4 production. Moreover, the production rate of CH_4

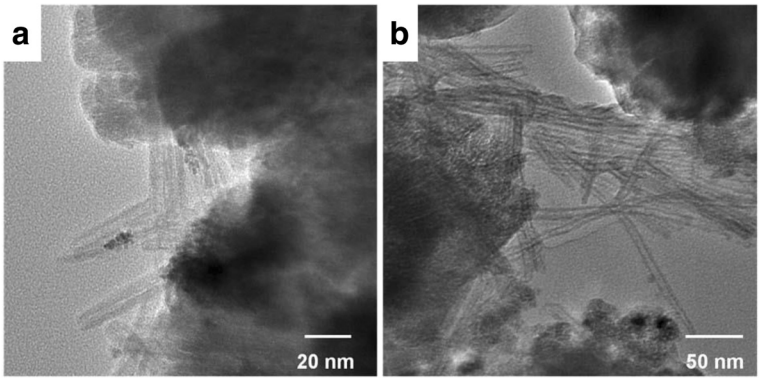

Fig. 6 TEM images of Pt loaded TS1 (**a**) and Pd loaded TS1 (**b**)

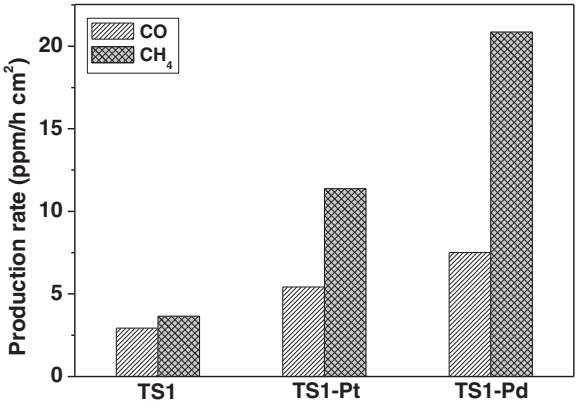

Fig. 7 Photocatalytic production rate of CH_4 and CO on TS1, TS1-Pt, and TS1-Pd

and CO increased 4.7 times and 1.6 times on TS1-Pd than TS1, implying that loading Pd nanoparticles on TS1 film is favorable to improve the selectivity of CO_2 phtoreduction to CH_4.

Conclusions

In summary, $TiO_2/SrTiO_3$ heterojunction network films were prepared successfully by hydrothermal method using nanotube titanic acid film (NTA) as the precursor. In the basic reaction process, part of NTA reacted with $SrCl_2$ to form $SrTiO_3$ naocubes, and the residues transformed to rutile TiO_2. As prolonging the reaction time to 2 h, NTA transformed to $SrTiO_3$ naocubes completely. The $TiO_2/SrTiO_3$ heterojunctions obtained at 1 h exhibit the best photocatalytic performance for the photoreduction of CO_2. The increased photocatalytic activity can be responded by the enhanced charge separation derived from the coupling effect the TiO_2 and $SrTiO_3$ components, large surface area (BET) and strong adsorption ability of TS1 network porous film. In addition, the photoreduction activity of CO_2 to CH_4 increased from 3.67 to 11.37 and 20.83 ppm/h cm^2 when Pt and Pd loaded on TS1 film. Especially, Pd also played the important role to increase the selectivity of photoreduction CO_2 to CH_4.

Competing interests

The authors declare that they have no competing interests.

Authors' contributions

YB and LZ carried out the total experiment. CL and JY participated in the date analysis. QL supervised the project, and provided the facilities and discussions related to them. All authors read and approved the final manuscript.

Acknowledgements

The authors gratefully acknowledge the support of the National Natural Science Foundation of China (Nos. 21103042 and 21471047), and Program for Science & Technology Innovation Talents in University of Henan Province (No. 15HASTIT043).

Received: 1 July 2015 Accepted: 19 August 2015
Published online: 28 August 2015

References

1. Mori K, Yamashita H, Anpo M. Photocatalytic reduction of CO_2 with H_2O on various titanium oxide photocatalysts. RSC Adv. 2012;2:3165–72.
2. Song CS. Global challenges and strategies for control, conversion and utilization of CO_2 for sustainable development involving energy, catalysis, adsorption and chemical processing. Catal Today. 2006;115:2–32.
3. Sakakura T, Choi JC, Yasuda H. Transformation of carbon dioxide. Chem Rev. 2007;107:2365–87.
4. Aresta M, Dibendetto A. Utilisation of CO_2 as a chemical feedstock: opportunities and hallenges. Dalton Trans. 2007;28:2975–92.
5. Centi G, Perathoner S. Opportunities and prospects in the chemical recycling of carbon dioxide to fuels. Catal Today. 2009;148:191–205.
6. Ma J, Sun NN, Zhang XL, Zhao N, Xiao FK, Wei W, et al. A short review of catalysis for CO_2 conversion. Catal Today. 2009;148:221–31.
7. Hoffmann MR, Martin ST, Choi WY, Bahemann DW. Environmental application of semiconductor photocatalysis. Chem Rev. 1995;95:69–96.
8. Chen XB, Mao SS. Titanium dioxide nanomaterials: synthesis, properties, modifications, and applications. Chem Rev. 2007;107:2891–959.
9. Fujishima A, Zhang X, Tyrk DA. TiO_2 photocatalysis and related surface phenomena. Surf Sci Report. 2008;63:515–82.
10. Bavykin DV, Walsh FC. Elongated titanate nanostructures and their applications. Eur J Inorg Chem. 2009;8:977–97.
11. Ghicov A, Schmuki P. Self-ordering electrochemistry: a review on growth and functionality of TiO_2 nanotubes and other self-aligned MO*x* structures. Chem Commun. 2009;20:2791–808.
12. Shankar K, Basham JI, Allam NK, Varghese OK, Mor GK, Feng XJ, et al. Recent advances in the use of TiO_2 nanotube and nanowire arrays for oxidative photoelectrochemistry. J Phys Chem C. 2009;113:6327–59.
13. Li QY, Kako T, Ye JH. PbS/CdS nanocrystal-sensitized titanate network films: enhanced photocatalytic activities and super-amphiphilicity. J Mater Chem. 2010;20:10187–92.
14. Chen YB, Wang LZ, Lu GQ, Yao XD, Guo LJ. Nanoparticles enwrapped with nanotubes: A unique architecture of CdS/titanate nanotubes for efficient photocatalytic hydrogen production from water. J Mater Chem. 2011;21:5134–41.
15. Chen YB, Guo LJ. Highly efficient visible-light-driven photocatalytic hydrogen production from water using $Cd_{0.5}Zn_{0.5}S$/TNTs (titanate nanotubes) nanocomposites without noble metals. J Mater Chem. 2012;22:7507–14.
16. Shi JW, Guo LJ. ABO_3-based photocatalysts for water splitting. Pro Nat Sci: Mater Int. 2012;22:592–615.
17. Scaife DE. Oxide semiconductors in photoelectrochemical conversion of solar energy. Solar Energ. 1980;25:41–54.
18. Wang JS, Yin S, Sato T. Characterization and evaluation of fibrous $SrTiO_3$ prepared by hydrothermal process for the destruction of NO. J Photochem Photobiol A: Chem. 2007;187:72–7.
19. Zhang SC, Liu JX, Han YX, Chen BC, Li XG. Formation mechanisms of $SrTiO_3$ nanoparticles under hydrothermal conditions. Mater Sci Eng B. 2004;110:11–7.
20. Cao TP, Li YJ, Wang CH, Shao CL, Liu YC. A facile in situ hydrothermal method to $SrTiO_3/TiO_2$ nanofiber heterostructures with high photocatalytic activity. Langmuir. 2011;27:2946–52.
21. Yang JJ, Jin ZS, Wang XD, Li W, Zhang JW, Zhang SL, et al. Study on composition, structure and formation process of nanotube $Na_2Ti_2O_4(OH)_2$. Dalton Trans. 2003;20:3898–901.
22. Xie J, Ji TH, Ouyang XH, Xiao ZY, Shi HJ. Preparation of SrTiO3 nanomaterial from layered titanate nanotubes or nanowires. Solid State Commun. 2008;147:226–9.
23. Zhang J, Bang JH, Tang CC, Kamat PV. Tailored $TiO_2 – SrTiO_3$ heterostructure nanotube arrays for improved photoelectrochemical performance. ACS Nano. 2010;4:387–95.
24. Huang JR, Tan X, Yu T, Zhao L, Hu WL. Enhanced photoelectrocatalytic and photoelectrochemical properties by high-reactive $TiO_2/SrTiO_3$ hetero-structured nanotubes with dominant {001} facet of anatase TiO_2. Electrochim Acta. 2014;146:278–87.
25. Li QY, Xing YY, Li R, Zong LL, Wang XD, Yang JJ. AgBr modified TiO_2 nanotube films: highly efficient photo-degradation of methyl orange under visible light irradiation. RSC Adv. 2012;2:9781–5.

26. Velmurugan R, Sreedhar B, Swaminathan S. Nanostructured AgBr loaded TiO_2: an efficient sunlight active photocatalyst for degradation of reactive Red 120. Chem Central J. 2011;5:46.
27. Li QY, Li R, Zong LL, He JH, Wang XD, Yang JJ. Photoelectrochemical and photocatalytic properties of Ag-loaded $BaTiO_3/TiO_2$ heterostructure nanotube arrays. Int J Hydrogen Energy. 2013;38:12977–83.
28. Li R, Li QY, Zong LL, Wang XD, Yang JJ. $BaTiO_3/TiO_2$ heterostructure nanotube arrays for improved photoelectrochemical and photocatalytic activity. Electrochim Acta. 2013;91:30–5.
29. Lu DD, Zhang M, Zhang ZH, Li QY, Wang XD, Yang JJ. Self-organized vanadium and nitrogen co-doped titania nanotube arrays with enhanced photocatalytic reduction of CO_2 to CH_4. Nanosca Res Lett. 2014;9:272.
30. Li QY, Zong LL, Li C, Yang JJ. Photocatalytic reduction of CO_2 on MgO/TiO_2 nanotube films. Appl Surf Sci. 2014;314:458–63.